Journal of Physics B: Atomic, Molecular and Optical Physics

Combined effect of non-linear optical and collisional processes on absorption saturation in a dense rubidium vapour

OPEN ACCESS
IOP Publishing
Journal of Physics B: Atomic, Molecular and Optical Physics
J. Phys. B: At. Mol. Opt. Phys. **53** (2020) 125402 (9pp)
https://doi.org/10.1088/1361-6455/ab7fc2

Combined effect of non-linear optical and collisional processes on absorption saturation in a dense rubidium vapour

A J van Lange[1], P van der Straten and D van Oosten

Debye Institute for Nanomaterials Science and Center for Extreme Matter and Emergent Phenomena, Utrecht University, Princetonplein 5, 3584 CC Utrecht, The Netherlands

E-mail: a.j.vanlange@uu.nl

Received 10 January 2020, revised 5 March 2020
Accepted for publication 13 March 2020
Published 27 May 2020

Abstract

We study non-linear absorption of intense monochromatic light through a dense natural rubidium (Rb) vapour. We measure transmission through a 10 cm long heated vapour cell for atom densities up to $3 \times 10^{19}\,\mathrm{m}^{-3}$ and saturation parameters up to 10^4, for linear and circular polarisation, close to resonance on the ^{87}Rb D_2 $F = 1 \rightarrow F' = 0, 1, 2$ transition. The strong absorption at low intensity is frustrated by an interplay of optical non-linearities (saturation and optical pumping) and non-linear effects due to the high atom density (collisional broadening and collisional depumping). To understand the results of the transmission measurements, we developed a model that incorporates these non-linear effects into the optical absorption. The model takes into account the absolute line strengths of all transitions from both hyperfine levels of the ground state of both isotopes of naturally abundant Rb. Doppler and collisional broadening are included in the Voigt profiles for the resonances. We show the effect of each of the non-linear processes on the calculation results of the model, and from comparison with experiment we conclude that all non-linear effects are necessary for a quantitative agreement.

Keywords: absorption, non-linear optics, saturation, optical pumping, collision broadening, atomic collision rate, dense rubidium gas

(Some figures may appear in colour only in the online journal)

1. Introduction

The study of optical properties of dense atomic vapours has resulted in the observation of fascinating non-linear effects on the propagation of light through such media [1]. An originally opaque dense vapour becomes transparent when excited with an intense control beam of laser light [2, 3]. This electromagnetically induced transparency (EIT) is performed in various schemes with resonant [4, 5] or off-resonant light [6, 7] and is applied in all-optical switching techniques [8–10]. An extreme way of controlling the propagation is in slow light experiments, in which the group velocity of the light is reduced by several orders of magnitudes compared to the speed of light in vacuum [11, 12]. In dense atomic vapours the velocity reduction has a broad bandwidth, making them suitable for slowing down picosecond pulses [13] and delaying nanosecond pulses by tens of pulse widths in a tunable all-optical delay line [14–16]. The dramatic reduction of speed to almost zero sparked research into storing light pulses in dense alkali vapours [17–21], which shows great promise in quantum network communication and synchronisation [22, 23].

In recent years focus has been on propagation through extremely dense vapours. In heated rubidium millicells, the transmission at low intensity was demonstrated to undergo collisional broadening [24, 25]. At frequencies below resonance and at high atomic densities, the propagation of the optical field

[1] Author to whom any correspondence should be addressed.

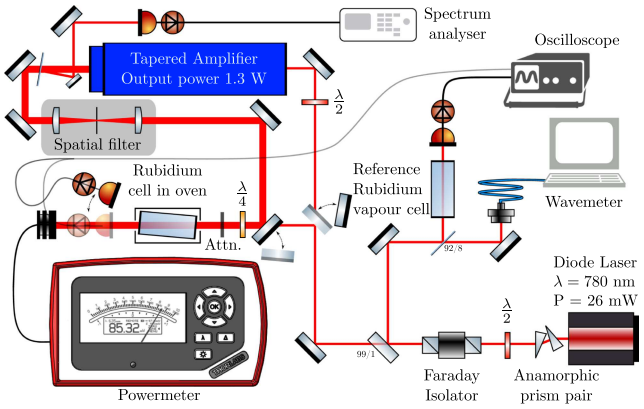

Figure 1. Schematic of the setup in two configurations: solid optical elements for high power measurements on the power metre, semi-transparent optical elements for low power calibration measurements on the oscilloscope. Important components in the setup are the TuiOptics DL-100 light source, Toptica BoosTA Tapered amplifier, HighFinesse WS-6 wavemeter and the Rode & Schwarz FSL6 spectrum analyser.

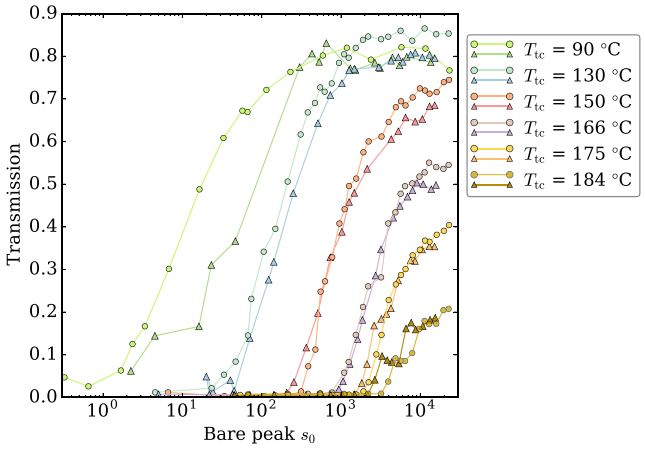

Figure 2. Transmission for circular (circles) and linear (triangle) polarisation for different cell temperatures. The bare peak saturation parameter is given by I_{peak}/I_s, where $I_{peak} = 2P_{in}/(\pi w_0^2)$ and I_s is 1.6 (2.5) mW cm^{-2} for circular (linear) polarisation. Transmission is measured at $\omega = 384\,234\,576$MHz (4170 MHz detuning in table 1), the transition strength weighted average of the ^{87}Rb $F = 1 \rightarrow F' = 0, 1, 2$ manifold. Temperatures are measured by a thermocouple.

was found to mimic the time evolution of a 2D-Bose gas with repulsive interactions [26, 27].

In the understanding of the effects of the experiments above, a proper description of the absorptive and refractive properties of the medium is pivotal. For specific ranges in intensity, atom density and detuning, these properties have been reported in earlier work: absorption has been studied at low laser intensities for high vapour densities [24, 28, 29], absorption with optical pumping at medium intensities [30–33], and absorption and refraction at high intensity and high atom density for large detunings [26, 34]. We capture these properties in a comprehensive model applicable over the whole range of detunings, saturation parameters and atomic densities. This makes the model suitable for all of the above mentioned areas of research. The principles of the model are applicable to any transition in an atomic vapour. We validate our model by comparing it to transmission measurements in a dense Rb vapour at high intensities close to resonance.

First we describe our experimental setup and present the measured on-resonance transmission curves as a function of saturation parameters up to 2.5×10^4 for temperatures from 60 to 130 °C. These results inspire us to construct a model to calculate the transmission, which includes the following non-linear effects: collisional broadening, optical pumping to the dark ground state, collisional depumping and saturation. We show the influence of each of the effects on the resulting transmission curve and show all effects are necessary to achieve quantitative agreement with the experimental results.

2. Experimental setup and transmission curves

The experimental setup to measure transmission through a heated cell containing rubidium with a natural isotope ratio is shown in figure 1. The 10 cm long vapour cell is wrapped with heating wires, isolated and placed in an aluminium heat shield. The temperature of the cell is controlled by the current through the wires and monitored by a thermocouple in direct contact with the cell wall.

Our light source is a continuous wave external cavity diode laser. An anamorphic prism pair ensures a circular beam and a 60 dB Faraday isolator prevents unwanted reflections from destabilising the laser. Part of the light is split off by a beam splitter for characterisation of the laser frequency using a wavemeter and through a spectroscopy cell at room temperature for reference. After the beam splitter the light can be sent directly through the heated cell for low intensity calibration measurements, in which the light is collected by a photodiode and recorded on the oscilloscope together with the signal from the reference cell. For high intensity measurements, the beam is amplified in a tapered amplifier (TA) to an output power of 1.3 W. Afterwards a small portion of the light is detected by a photodiode and analysed using an electronic spectrum analyser to ensure the diode laser has no multimode sidebands. Spatial filtering converts the elongated TA output mode into a Gaussian beam with a waist w_0 of 850 μm. At the entrance window of the heated cell the beam power is 500 mW, which can be attenuated to lower powers by absorptive neutral density filters just before cell entry. For circular polarisation measurements a quarter wave plate is placed in front of these attenuators. The transmission is collected and recorded by a power metre directly after the vapour cell.

The measured transmission for circular and linear polarisation at several cell temperatures is shown in figure 2. To avoid the possibility of self-focusing effects which occur above the resonance, transmission traces were taken slightly below resonance. The bare peak s_0 is determined by I_{peak}/I_s where $I_{peak} = 2P_{in}/(\pi w_0^2)$ and the saturation intensity I_s is 1.6 (2.5) mW cm^{-2} for circular (linear) polarisation. The sudden rise from zero to non-zero of the transmission suggests a saturation effect. At the highest experimental s_0 the transmission levels off to a value depending on the atom density. This suggests a non-linear effect in atom density.

3. Transmission model

The intensity of light propagating through the dense rubidium vapour is subject to the Lambert–Beer equation

$$\frac{\mathrm{d}I(\omega)}{\mathrm{d}z} = -\alpha(I,\omega)I(\omega), \tag{1}$$

where I is the intensity, z the propagation direction, ρ_{at} the atomic density and α the absorption coefficient. Refraction has a negligible effect in on-resonance experiments and is therefore not included in this treatment of the transmission.

To determine the absorption coefficient α we take into account all allowed transitions that make up the Rb D_2 line [29]. For the correct transition frequencies of these transitions, we calculate the hyperfine frequency shifts for the ground state and the excited state of both isotopes [35, 36]. Table 1 shows the resulting frequencies for all transitions from $F_g = i$ to $F_e = j$ in the D_2 manifold. The frequencies ω_0^{ij} are listed with respect to the excitation frequency of ^{85}Rb, as determined without hyperfine splitting. There we also list the transition strength coefficients R^{ij} with respect to the cycling transition. The absorption coefficient α is calculated by summing over all the allowed transitions as

$$\alpha(\omega, I) = \frac{3\lambda^2}{2\pi} \sum_{\text{isotopes}} \sum_{i} \sum_{j=i-1}^{i+1} \rho_i R^{ij} V(\omega - \omega_0^{ij}, s_0^{ij}), \tag{2}$$

where $\frac{3\lambda^2}{2\pi}$ is the light-atom scattering cross-section for a two-level system, λ is the transition wavelength, ρ_i is the density of atoms in ground state i, and $s_0^{ij} = R^{ij} I / I_{\mathrm{s}}$ is the transition specific saturation parameter with I_{s} the saturation intensity for the cycling transition. $V(\delta, s_0)$ is the Voigt profile, which is a convolution of the Doppler profile and a (collisionally and power) broadened Lorentz profile.

Use of the Voigt profile is required, because at high intensities power broadening makes the broadened Lorentz width comparable to the Doppler width and the Voigt profile thus ensures the models validity over a large range of detunings: from far above to far below the Doppler width (figure 3).

In the convolution only the axial velocity distribution needs to be taken into account, because the velocity distributions in different directions are decoupled. The Doppler integral for the Voigt profile is thus

$$V(\delta, s_0^{ij}) = \frac{1}{\sqrt{2\pi} v_{\mathrm{th}}} \int_{-\infty}^{\infty} \mathrm{d}v\, \mathrm{e}^{-\frac{1}{2}\frac{v^2}{v_{\mathrm{th}}^2}} \frac{1}{1 + (2\delta(v)/\gamma)^2 + s_0^{ij}}, \tag{3}$$

where $v_{\mathrm{th}} = \sqrt{k_{\mathrm{B}} T / m}$, γ is the linewidth of the transition and the detuning δ is dependent on the atom velocity v as $\delta(v) = \delta_0 - v/\lambda$, with δ_0 the original detuning of the excitation and λ the transition wavelength.

The Voigt profiles are obtained using the real part of the Faddeevva function $w(z)$, for which we use the python implementation `scipy.special.wofz`, as follows:

$$V(\delta_0, s_0; v_{\mathrm{th}}, \gamma) = \int_{-\infty}^{\infty} \mathrm{d}v' \frac{\frac{1}{\sqrt{2\pi} v_{\mathrm{th}}} \mathrm{e}^{-\frac{1}{2}\frac{v'^2}{v_{\mathrm{th}}^2}}}{1 + \left(2(\delta_0 - v'/\lambda)/\gamma\right)^2 + s_0}$$

Table 1. Transition frequencies and transition strengths for the D_2-lines of rubidium. Frequencies are listed with respect to the excitation frequency without hyperfine splitting of ^{85}Rb (384 230 406.373 MHz). Transition strengths with respect to the cycling frequency transition strength.

F_g (=i)	F_e (=j)	$\omega_0^{ij} - \omega_0$ (MHz)	R^{ij}
^{85}Rb	1	−1378.068 75	0
$F_g = 3$	2	−1348.754 75	$\frac{10}{27}$
	3	−1285.373 75	$\frac{35}{27}$
	4	−1164.633 75	$\frac{81}{27}$
^{85}Rb	1	1657.661 25	1
$F_g = 2$	2	1686.975 25	$\frac{35}{27}$
	3	1750.356 25	$\frac{28}{27}$
	4	1871.096 25	0
^{87}Rb	0	−2787.4225	0
$F_g = 2$	1	−2715.0995	$\frac{1}{6}$
	2	−2557.9295	$\frac{5}{6}$
	3	−2290.8745	$\frac{14}{6}$
^{87}Rb	0	4047.2575	$\frac{2}{6}$
$F_g = 1$	1	4119.5825	$\frac{5}{6}$
	2	4276.7525	$\frac{5}{6}$
	3	4543.8075	0

$$= \frac{\pi\gamma}{2\sqrt{1+s_0}} \frac{\lambda}{\sqrt{2\pi} v_{\mathrm{th}}} \mathrm{Re}[w(z)], \tag{4}$$

where

$$z = \frac{\delta_0 + i\frac{1}{2}\gamma\sqrt{1+s_0}}{\sqrt{2} v_{\mathrm{th}}/\lambda}. \tag{5}$$

The homogeneous linewidth γ is broadened at high densities due to collisional broadening and is given by $\gamma = \gamma_0 + \beta\rho_{\mathrm{at}}$. For the rubidium D_2 line the natural linewidth $\gamma_0 = 6.06$MHz and the collisional broadening coefficient $\beta = (1.10 \pm 0.17) \times 10^{-19}\,\mathrm{m}^3\,\mathrm{MHz}$ is determined in previous experimental work [25, 37]. The saturation parameter is defined as $s_0 = 2\Omega^2/\gamma^2$ with Ω the Rabi frequency, and since the linewidth broadening is a homogeneous effect, the bare peak saturation parameter needs to be adjusted by a factor γ^2/γ_0^2 in the dense Rb vapour.

The response of the medium to a beam of light with intensity I and frequency ω, now only depends on the temperature and the density. The density can be expressed as a function of temperature by [38]

$$\rho_{\mathrm{at}}(T) = \frac{p}{k_{\mathrm{B}} T}, \quad \text{with } \log_{10}(p) = 5.0057 + 4.312 - 4040/T, \tag{6}$$

where p is the vapour pressure and k_{B} is the Boltzmann constant. We measure the temperature on a particular part of the cell wall, but the atoms in the vapour cell thermalise to the coldest point of the cell. Therefore we perform a calibration to relate the equilibrium temperature of the atoms to the measured temperature of the cell wall.

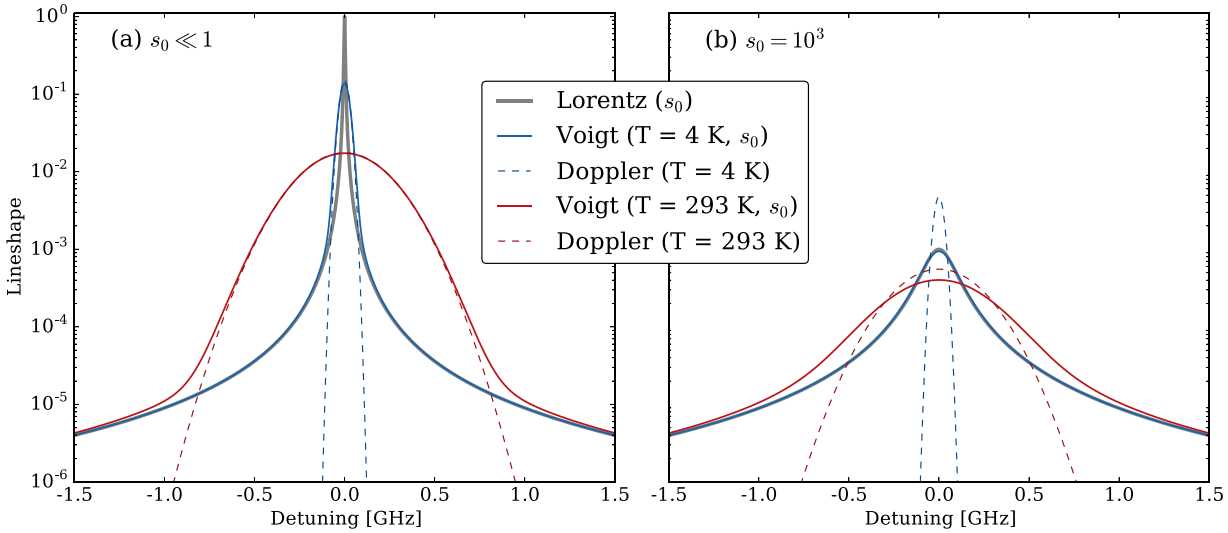

Figure 3. Lorentz, Doppler and Voigt profiles for a single resonance line for (a) low saturation ($s_0 \ll 1$) and (b) high saturation ($s_0 = 10^3$). The Doppler widths for $T = 4$ K and $T = 293$ K given by $\delta_{\text{th}} = v_{\text{th}}/\lambda$ are 25 and 215 MHz. The Doppler profiles are scaled with $\pi\gamma/(2\sqrt{1+s_0})$ for proper comparison with the Voigt profiles. (a) At low saturation the Voigt profile resembles the Doppler profile at low detuning $|\delta| \leqslant 4\delta_{\text{th}}$ and the Lorentz profile at high detuning. The Voigt profile is required for calculation over the full range of detuning. (b) At high saturation the power broadened Lorentz width becomes comparable to the Doppler width at room temperature and the Voigt profile is the only accurate description over a large range of detunings.

4. Atom temperature calibration

To calibrate the atom temperature in the vapour cell, we measure the transmission spectra of a low intensity beam and fit the spectra using the model above (figure 4). The transmission signals from the heated cell and the reference cell are recorded on an oscilloscope. In this experiment the laser frequency is varied by modulating the current through the laser diode. Intensity changes due to this modulation are compensated for by fitting the background slope of the reference signal to second order in detuning.

As the transmission in a dense rubidium vapour is zero for large parts of the spectrum around the resonances, the frequency axis is calibrated by fitting the reference signal with our calculation model as a function of temperature. The result for room temperature measurements in figure 4 shows a good fit with a temperature of 18.9 °C. The fit procedure was confirmed to produce undiscernible results for a fit function with pure Doppler profiles, which is equally appropriate for low intensity and a fitting range within a few Doppler widths of the resonances. We also verified the fit function by reproducing the spectral fits of transmission through high density vapours in millicells [39].

At higher temperatures the transmission is zero over a large range around the resonances. The parts of the spectrum useful for fitting are therefore located in the wings, where only the Voigt-profiles are valid. The fits in figure 4 show good agreement with the data. The table shows the relation between the temperature obtained from the spectral fit (T_{sp}) and the temperature measured by the thermocouple (T_{tc}). We use a linear fit to assign a spectral temperature to all the temperatures at which transmision is measured in figure 2 and find the relation

$$T_{\text{sp}} = (5.9 \pm 4.6)\,^{\circ}\text{C} + (0.636 \pm 0.028)\,T_{\text{tc}}. \tag{7}$$

This equation provides a good working value for the spectral temperature to calculate the transmission for high density and high temperature conditions of our measurements, despite the uncertainty in the relation.

5. Saturation and optical pumping

Even though the above model includes saturation and power broadening, it is not yet suitable to use at high intensities, where optical pumping comes into play. In optical pumping a fraction of the atoms is pumped into an optical dark state, leaving fewer atoms available for excitation in the bright state. The effect is most prominent, when pumping is on resonance with one of the transitions from a particular ground hyperfine states. The strong laser beam pumps atoms from the resonant, bright hyperfine ground state to the excited state, from which they have a possibility of falling into the other, dark hyperfine ground state.

The process is depicted in the Jablonski diagram in figure 5(a) and can be described by Einstein rate equations. The pumping rate from ground state i to the combined excited level e is given by

$$\Gamma_{ie} = \frac{2\pi\gamma}{2}\sum_j V(\delta^{ij}, s_0^{ij}), \tag{8}$$

where $\delta^{ij} = \omega - \omega^{ij}$. The chance to fall back into the lower (upper) hyperfine ground state is given by the branching ratio br_{ei}, 1/2 (1/2) for ^{85}Rb and 4/9 (5/9) for ^{87}Rb [36].

Since we work at high atomic densities, collisions occur frequently. The collisional depumping rates Γ_{12} and Γ_{21}, which redistribute the population over the ground states, therefore need to be included. The rates are not equal because of a difference in multiplicity m_i and are given by

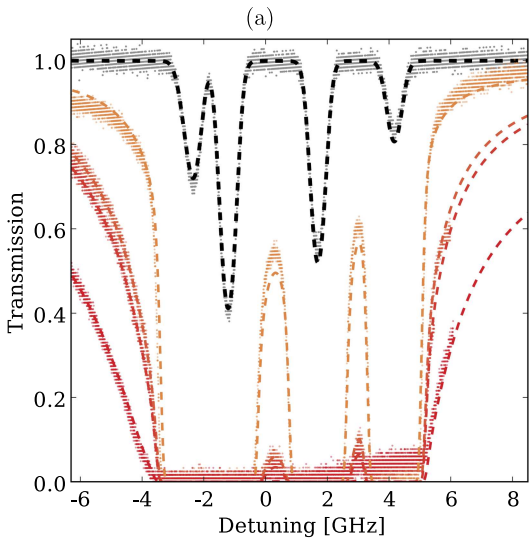

(b)

T_{tc} [°C]	T_{sp} [°C]	$\rho_{at}(T)$ [$\times 10^{19}$m^{-3}]
166	105.7 ± 0.4	0.82 ± 0.02
183	124.6 ± 1.0	2.62 ± 0.15
188	127.0 ± 1.2	2.89 ± 0.20
202	136.2 ± 1.2	4.93 ± 0.31
		[$\times 10^{15}$m^{-3}]
19	18.88 ± 0.02	6.56 ± 0.01

Figure 4. (a) Measured transmission spectra for cell temperatures of 166 to 202 °C (coloured dots). The reference spectrum at room temperature (grey dots) is fitted with Doppler (blue line) and Voigt profile (black dashed) and determines the frequency-axis for the high temperature spectra. Coloured dashed line are the Voigt fits for the corresponding higher temperature measurements. (b) Temperatures and densities resulting from the fit for several measured cell temperatures.

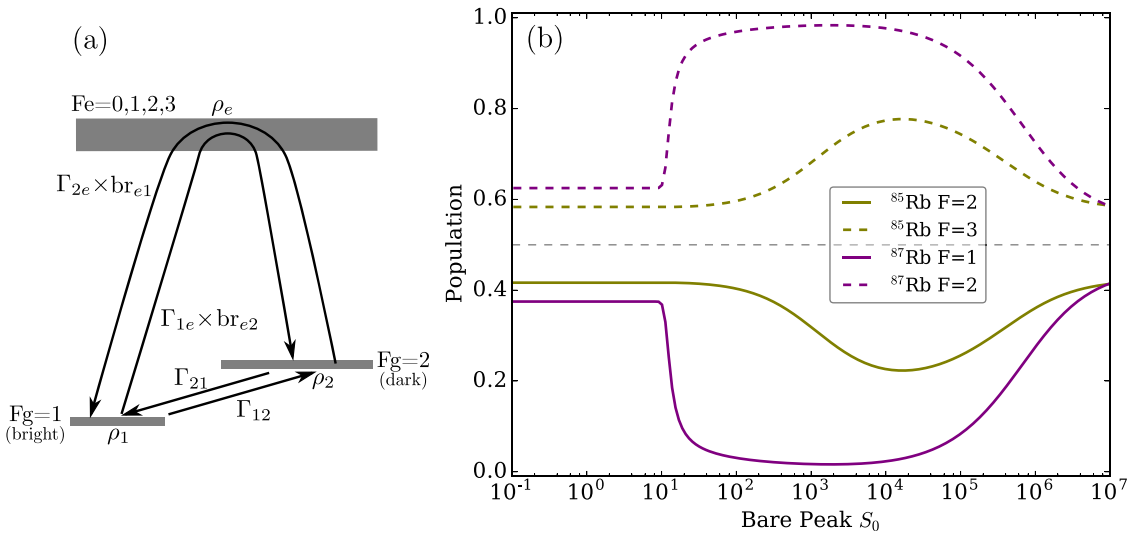

Figure 5. (a) Schematic energy diagram for the optical pumping mechanism for ^{87}Rb. The bright and dark state refer specifically to the case of pumping on resonance with the ^{87}Rb $F_g = 1$ state, as used in the experiment and in calculations in (b). (b) Steady state population of the ground states for pumping on resonance with the ^{87}Rb $F_g = 1$ state as function of s_0. Above $s_0 \simeq 10$ optical pumping becomes larger than collisional depumping and the population of the bright ground state is depleted severely.

$\Gamma_{12} = \Gamma_{\rm col}\frac{m_2}{m_1+m_2}$ and $\Gamma_{21} = \Gamma_{\rm col}\frac{m_1}{m_1+m_2}$. Here we have introduced the collision rate $\Gamma_{\rm col} = \rho_{\rm at} v_{\rm col}\sigma_{\rm col}$, where $v_{\rm col} = 2v_{\rm th}$ is the most probable interatomic speed and $\sigma_{\rm col}$ is the collisional cross section.

Collision rates and collisional cross sections specifically are notoriously difficult to determine and inherently specific for the process under investigation. Collision rates have been determined for ultracold Rb atoms in magnetic and magneto-optical traps [40] and spin relaxation and excitation-transfer collisions between Rb and buffer gases [41, 42], but not for the hyperfine ground state changing collision of concern here. To estimate this specific cross section we determine the relevant impact parameter by calculating the minimum distance between atoms for which the energy exchange exceeds the hyperfine splitting of the ^{87}Rb ground state. This is the largest energy difference to be overcome for a hyperfine state change, which can therefore occur during a collision between any two atoms. The energy transfer for a given impact parameter depends on the type of interaction involved in the collision. The collision between identical atoms is described by a van der Waals potential C_6/R^6, for which the C_6 coefficient of Rb is 4.47×10^3 in atomic units [43, 44]. The estimate for the impact parameter b in this case is 1.43 nm and the collisional cross section is $\sigma_6 = \pi b^2 = 6.42\,\text{nm}^2$, which is of the same order of magnitude as the total elastic scattering cross section $Q = 23.6\,\text{nm}^2$ [40]. Dipole–dipole-type collisions,

with van der Waals potenial C_3/R^3, between excited and ground state can be neglected, because the occupation of the excited state is severely reduced by optical pumping up to saturation parameters in the order of 10^5, when the power broadening becomes of the order of the ground state hyperfine splitting.

We solve the Einstein rate equations for the above values and find the populations of the ground states of both isotopes shown in figure 5(b). The population of the bright ground state reduces strongly when the pumping laser is on resonance with this bright state. We also notice this effect in the transmission spectra. The drop in bright state population strongly enhances the transmission.

The populations we find are the ingredient for a final adjustment of our treatment of saturation. The transition-specific saturation parameter depends on the occupation of the excited state in question. At high intensities, the contribution to the excitation from the other ground state cannot be neglected anymore, as due to power broadening their absorption overlaps significantly. The transition-specific s_0^{ij} will therefore also include a contribution from the other ground state, which we write formally as a sum over all other ground states as

$$s_0^{ij} = s_0 R^{ij} + s_0 \sum_{k \neq i} R^{kj} \frac{\rho_k}{\rho_i} \frac{1}{1 + (2\delta^{kj}/\gamma^{kj})^2}, \tag{9}$$

where $\gamma^{kj} = \gamma\sqrt{1 + R^{kj} s_0}$ is the transition specific power broadened linewidth. With the saturation parameters s_0^{ij} dependent on the populations ρ_i, and the populations dependent on the saturation parameter, the model needs to calculate these quantities in an iterative procedure, for which convergence is reached after 3 iterations.

6. Transmission at resonance

The interplay of all the non-linear processes described above has a particularly intriguing effect on the transmission at resonance. We apply our model to the transmission at the ^{87}Rb $F = 1 \rightarrow F' = 0, 1, 2$ transition over a wide range of saturation parameters s_0 for one typical temperature (111 °C). To accurately describe the experimental conditions, we simulate the propagation of a Gaussian beam by discretizing the Gaussian in 20 regions and propagating these regions in parallel in 10 steps. For comparison with experimentally obtained transmission, we compensate for losses from passing the windows of the cell by a factor of $\sqrt{0.85}$ at each window. This factor is chosen to match the measured transmission of 85% far off-resonance at $\delta = 20$ GHz. To illustrate the influence of the separate non-linear effects, we turn the effects on one-by-one, as shown in figure 6.

We start with the curve taking into account only saturation (solid line). The threshold at which transmission becomes non-zero is at $s_0 \simeq 10^5$, far from the experimentally observed value of $\simeq 10^3$, and the curve has no intermediate plateau. With the introduction of optical pumping (dashed-dotted line) a plateau appears for $s_0 < 10^5$, caused by the near depletion of the bright state. As there are no collisions to repopulate the bright state, the bright state is only repopulated by the reverse optical pumping from the dark state, which is much weaker because it is much further detuned. In the steady state solution the population of the bright state is therefore only a few percent (see figure 5(b)), which is nevertheless responsible for significant absorption. As this fraction of the atom density is stable for all s_0 (up to $s_0 \sim 10^5$), the amount of absorption and thus the level of transmission is determined by the atom density. The height of this plateau is therefore dependent on the atom density, in accordance with experimental observations.

With the introduction of collisions into our model (dotted line) the curve resembles the shape of the measurement data, as the effect of optical pumping are suppressed by collisional depumping for $\Gamma_{21} > \Gamma_{1e}\mathrm{br}_{e2}$. This criterion determines the threshold, where the transmission becomes non-zero. For the collisional rate estimated above, this occurs at $s_0 \sim 20$ and is not in agreement with the experiments. We therefore adjust the collision rate through the estimated collisional cross section such that the model matches all of our measurements simultaneously.

The collisional cross section is an intrinsic property of the Rb vapour and independent on the atom density and temperature, for the range of temperatures that we have explored. The optimum value for the cross section is therefore best recovered by simultaneously matching our model to *all* of the measurements in figure 2, using a single value of the cross section as the only free parameter, for the temperature relation in equation (7). The resulting curves are judged on retrieval of the correct curve slopes and the correct thresholds for the value of s_0 at which transmission first becomes non-zero. The results of this procedure for are shown in figures 6 and 7 for an optimum value of $\sigma_{\mathrm{col}} = 67\,\mathrm{nm}^2$. In particular the correct slope for different temperatures and the correct threshold values for s_0 are captured. Note that this should not be interpreted as a measurement of σ_{col}, as the uncertainty in the coefficients of the temperature calibration leads to a large uncertainty in σ_{col}. The lower bound of the temperature yields an optimum for $\sigma_{\mathrm{col}} = 322\,\mathrm{nm}^2$, whereas the upper bound gives $\sigma_{\mathrm{col}} = 19\,\mathrm{nm}^2$. Since we are here concerned with the resulting optical properties, more accurate knowledge of T_{sp} and thus σ_{col} is not required.

The model only deviates from the measurement at $T_{\mathrm{tc}} = 90\,°\mathrm{C}$, at which the spectral temperature is more uncertain, as it is far away from the calibration points (19, 166, 183, 188 and 202 °C) for the linear temperature fit of equation (7). The performed calibration was mainly aimed at high temperatures, where non-linear effects are most prominent. But more importantly, at these intermediate temperatures the optical pumping scheme of figure 5, which neglects magnetic sublevels and hyperfine states of the excited state, might be an oversimplification. This notion is supported by the difference in behaviour for different polarisations, which is expected to happen when more subtle pumping effects including magnetic sublevels of the ground and excited states become important. For higher temperatures the model accurately describes the non-linear transmission through a dense rubidium vapour for $s_0 < 10^4$.

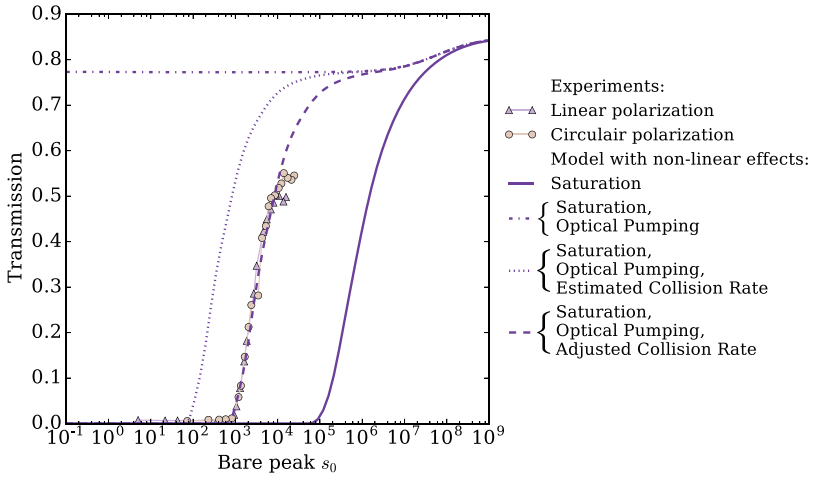

Figure 6. Transmission measurements at $T_{\mathrm{tc}} = 166\,^{\circ}\mathrm{C}$ and calculation at $T_{\mathrm{at}} = 111\,^{\circ}\mathrm{C}$ (from equation (7)). In the plots the non-linear effects are turned on one-by-one. With only saturation turned on (solid line) the threshold s_0, where transmission becomes non-zero, is too high. With the introduction of optical pumping (dash-dotted line) an the atom density dependent plateau appears and transmission stays non-zero even for low s_0. Addition of collisions to the model introduces a new theshold value for non-zero transmission, which is too low for the estimated collisional cross section of 6.4 nm^2. With a collision rate of 67 nm^2, adjusted to fit our measurements, the model (dashed line) shows the correct threshold value of $s_0 \simeq 10^3$. This collisional cross section is chosen to match the calculations to all experiments in figure 7 simultaneously.

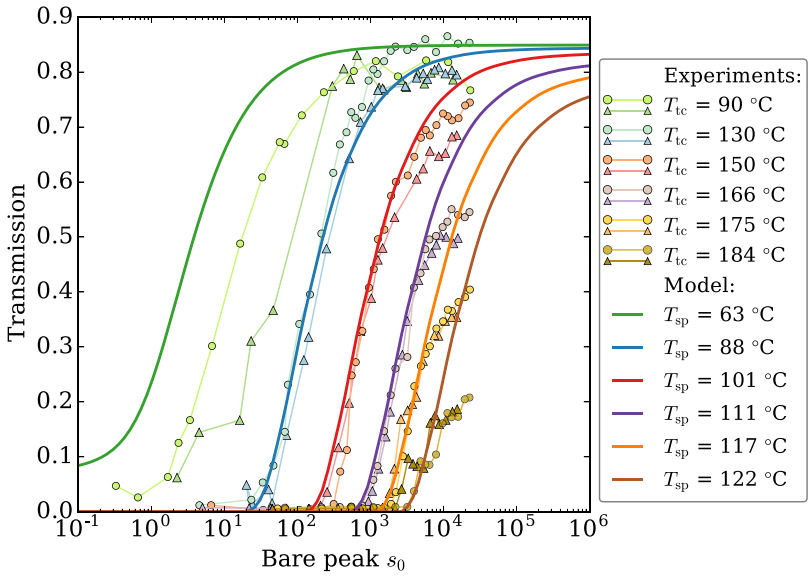

Figure 7. Transmission for circular (circles) and linear (triangle) polarisation for different cell temperatures. Transmission is measured at $\omega = 384\,234\,576$MHz, which is 4170 MHz detuning in table 1, the weighted average of the ^{87}Rb $F = 1 \rightarrow F' = 0, 1, 2$ manifold. Temperatures measured by the thermocouple T_{tc} and the corresponding temperatures T_{sp} from absorption spectrum analysis (equation (7)) are used as input temperature for the model calculations (solid lines). The collisional cross section is set to $\sigma_{\mathrm{col}} = 67$ nm^2.

For higher s_0 the effects of non-linear refraction and non-negligible population of the excited state need to be taken into account.

7. Conclusion

We developed a model to describe the absorption of a continuous light source in a dense rubidium vapour at high intensity. The model includes non-linear effects in intensity (optical pumping and saturation) and atomic density (collisional broadening and collisional depumping). The principles of the model are applicable to any transition in an atomic vapour. The model is particularly straight forward to transfer to the D_2 line of another alkali metal, as only values of the atomic properties need to be adjusted. We compare the results of our model to measurements of transmission through a 10 cm cell containing a dense vapour of a natural isotope mixture of rubidium. The transmission for light resonant with the highest line in the Rb D_2 manifold shows good agreement for saturation parameters $s_0 < 10^4$ and temperatures $90\,^{\circ}\mathrm{C} < T_{\mathrm{sp}} < 130\,^{\circ}\mathrm{C}$, when we assume a collisional cross section of $\sigma_{\mathrm{col}} = 67$ nm^2. We show that all the non-linear effects included in the model are essential to explain the characteristics of the transmission curves.

Acknowledgments

This work was performed with funding from NWO. The authors thank Paul Jurrius, Dante Killian and Cees de Kok for technical support.

ORCID iDs

A J van Lange https://orcid.org/0000-0003-0395-7476

Bibliography

[1] Paul S 2014 Light propagation through atomic vapours *J. Phys. B: At. Mol. Opt. Phys.* **47** 093001
[2] Harris S E 1997 Electromagnetically induced transparency *Phys. Today* **50** 36–42
[3] Fleischhauer M, Imamoglu A and Marangos J P 2005 Electromagnetically induced transparency: optics in coherent media *Rev. Mod. Phys.* **77** 633–73
[4] Harris S E and Yamamoto Y 1998 Photon switching by quantum interference *Phys. Rev. Lett.* **81** 3611–4
[5] Yan M, Rickey E G and Zhu Y 2001 Observation of absorptive photon switching by quantum interference *Phys. Rev.* A **64** 043807
[6] Scully M O 1991 Enhancement of the index of refraction via quantum coherence *Phys. Rev. Lett.* **67** 1855–8
[7] Scully M O and Fleischhauer M 1992 High-sensitivity magnetometer based on index-enhanced media *Phys. Rev. Lett.* **69** 1360–3
[8] Braje D A, Balić V, Yin G Y and Harris S E 2003 Low-light-level nonlinear optics with slow light *Phys. Rev.* A **68** 041801
[9] Zhang J, Hernandez G and Zhu Y 2007 All-optical switching at ultralow light levels *Opt. Lett.* **32** 1317–9
[10] Wu H, Xiao M and Gea-Banacloche J 2008 Evidence of lasing without inversion in a hot rubidium vapor under electromagnetically-induced-transparency conditions *Phys. Rev.* A **78** 041802
[11] Vestergaard Hau L, Harris S E, Dutton Z and Behroozi C H 1999 Light speed reduction to 17 metres per second in an ultracold atomic gas *Nature* **397** 594–8
[12] Slowe C, Ginsberg N S, Ristroph T, Goodsell A and Vestergaard Hau L 2005 Ultraslow light & Bose-Einstein condensates: two-way control with coherent light & atom fields *Opt. Photonics News* **16** 30–4
[13] Camacho R M, Pack M V, Howell J C, Schweinsberg A and Boyd R W 2007 Wide-bandwidth, tunable, multiple-pulse-width optical delays using slow light in cesium vapor *Phys. Rev. Lett.* **98** 153601
[14] Tanaka H, Niwa H, Hayami K, Furue S, Nakayama K, Kohmoto T, Kunitomo M and Fukuda Y 2003 Propagation of optical pulses in a resonantly absorbing medium: observation of negative velocity in Rb vapor *Phys. Rev.* A **68** 053801
[15] Vanner M R, McLean R J, Hannaford P and Akulshin A M 2008 Broadband optical delay with a large dynamic range using atomic dispersion *J. Phys. B: At. Mol. Opt. Phys.* **41** 051004
[16] Paul S, Bell N C, Cai Y, Adams C S and Hughes I G 2009 A gigahertz-bandwidth atomic probe based on the slow-light Faraday effect *Nat. Photon.* **3** 225–9
[17] Phillips D F, Fleischhauer A, Mair A, Walsworth R L and Lukin M D 2001 Storage of light in atomic vapor *Phys. Rev. Lett.* **86** 783–6
[18] Liu C, Dutton Z, Behroozi C H and Vestergaard Hau L 2001 Observation of coherent optical information storage in an atomic medium using halted light pulses *Nature* **409** 490–3
[19] Heinze G, Hubrich C and Halfmann T 2013 Stopped light and image storage by electromagnetically induced transparency up to the regime of one minute *Phys. Rev. Lett.* **111** 033601
[20] Wang G, Zhou W, Chen H-L, Xue Y, Wu J-H, Xu H-L and Gao J-Y 2016 Efficient light storage with reduced energy loss via nonlinear compensation in rubidium vapor *Laser Phys.* **26** 065201
[21] Katz O and Firstenberg O 2018 Light storage for one second in room-temperature alkali vapor *Nat. Commun.* **9** 1–6
[22] Schweickert L, Klaus D J, Namazi M, Cui G, Lettner T, Zeuner K D and Montana L S 2018 Electromagnetically induced transparency of on-demand single photons in a hybrid quantum network arXiv:1808.05921
[23] Siverns J D, Hannegan J and Quraishi Q 2019 Demonstration of slow light in rubidium vapor using single photons from a trapped ion *Sci. Adv.* **5** eaav4651
[24] Lee W, Bettles R J, Paul S, Adams C S and Hughes I G 2011 Absolute absorption on the rubidium D1 line including resonant dipole–dipole interactions *J. Phys. B: At. Mol. Opt. Phys.* **44** 195006
[25] James K 2013 Cooperative interactions in dense thermal Rb vapour confined in nm-scale cells *PhD Thesis* Durham University, Durham
[26] Šantić N, Fusaro A, Salem S, Garnier J, Picozzi A and Kaiser R 2018 Nonequilibrium precondensation of classical waves in two dimensions propagating through atomic vapors *Phys. Rev. Lett.* **120** 055301
[27] Fontaine Q, Bienaimé T, Pigeon S, Giacobino E, Bramati A and Glorieux Q 2018 Observation of the Bogoliubov dispersion in a fluid of light *Phys. Rev. Lett.* **121** 183604
[28] Shin S R and Noh H-R 2010 Analytic calculation of absorption spectra for doppler-broadened alkali-metal atoms at low laser intensity *J. Korean Phys. Soc.* **57** 325–8
[29] Paul S, Adams C, Chang G and Hughes I 2008 Absolute absorption on rubidium D lines: comparison between theory and experiment *J. Phys. B: At. Mol. Opt. Phys.* **41** 155004
[30] Stace T M and Luiten A N 2010 Theory of spectroscopy in an optically pumped effusive vapor *Phys. Rev.* A **81** 033848
[31] Shin S R and Noh H 2009 Effect of optical pumping on transmission spectra of rubidium *2009 Conf. on Lasers and Elecro Optics and the Pacific Rim Conf. on Lasers and Electro Optics*
[32] Lindvall T and Tittonen I 2007 Effect of optical pumping on alkali-atom Doppler-limited spectra *J. Mod. Opt.* **54** 2779–93
[33] Lindvall T and Tittonen I 2009 Interaction-time-averaged optical pumping in alkali-metal-atom Doppler spectroscopy *Phys. Rev.* A **80** 032505
[34] Paul S, Adams C S and Hughes I G 2009 Off-resonance absorption and dispersion in vapours of hot alkali-metal atoms *J. Phys. B: At. Mol. Opt. Phys.* **42** 175004
[35] Arimondo E, Inguscio M and Violino P 1977 Experimental determinations of the hyperfine structure in the alkali atoms *Rev. Mod. Phys.* **49** 31–75
[36] van der Straten P and Metcalf H 2016 *Atoms and Molecules Interacting with Light* (Cambridge: Cambridge University Press)
[37] Kondo R, Tojo S, Fujimoto T and Hasuo M 2006 Shift and broadening in attenuated total reflection spectra of the hyperfine-structure-resolved D_2 line of dense rubidium vapor *Phys. Rev.* A **73** 062504
[38] Alcock C B, Itkin V P and Horrigan M K 1984 Vapour pressure equations for the metallic elements: 298–2500 K *Can. Metall. Q.* **23** 309–13

[39] Lee W, Dalton T, Paul S, Adams C S and Hughes I G 2012 Measuring the Stokes parameters for light transmitted by a high-density rubidium vapour in large magnetic fields *J. Phys. B: At. Mol. Opt. Phys.* **45** 055001

[40] Beijerinck H C W 2000 Rigorous calculation of heating in alkali-metal traps by background gas collisions *Phys. Rev.* A **61** 033606

[41] Franz F A and Volk C 1976 Spin relaxation of rubidium atoms in sudden and quasimolecular collisions with light-noble-gas atoms *Phys. Rev.* A **14** 1711–28

[42] Beahn T J, Condell W J and Mandelberg H I 1966 Excitation-transfer collisions between rubidium and helium atoms *Phys. Rev.* **141** 83–7

[43] Derevianko A, Johnson W R, Safronova M S and Babb J F 1999 High-precision calculations of dispersion coefficients, static dipole polarizabilities, and atom-wall interaction constants for alkali-metal atoms *Phys. Rev. Lett.* **82** 3589–92

[44] Roberts J L, Claussen N R, Burke J P, Greene C H, Cornell E A and Wieman C E 1998 Resonant magnetic field control of elastic scattering in cold ^{85}Rb *Phys. Rev. Lett.* **81** 4